Available online at www.sciencedirect.com
ScienceDirect
Journal of Sound and Vibration 318 (2008) 1210–1229
JOURNAL OF SOUND AND VIBRATION
www.elsevier.com/locate/jsvi

A unified approach for analyzing static and dynamic behaviors of functionally graded Timoshenko and Euler–Bernoulli beams

X.-F. Li

Institute of Mechanics and Sensor Technology, School of Civil Engineering and Architecture, Central South University, Changsha, Hunan 410083, China

Received 25 July 2007; received in revised form 10 January 2008; accepted 26 April 2008
Handling Editor: L.G. Tham
Available online 18 June 2008

Abstract

This paper presents a new unified approach for analyzing the static and dynamic behaviors of functionally graded beams (FGB) with the rotary inertia and shear deformation included. As two special cases, the Euler–Bernoulli and Rayleigh beam theories can be analytically reduced from the Timoshenko beam theory. All material properties are arbitrary functions along the beam thickness. A single fourth-order governing partial differential equation is derived and all physical quantities can be expressed in terms of the solution of the resulting equation. The static result of deflection and stress distribution is presented for a cantilever FGB. Furthermore, two branches of flexural waves propagating in FGB are obtained with different wave speeds. The higher wave speed disappears when the effects of neither the rotary inertia nor shear deformation are considered. Free vibration of an FGB is analyzed and the frequency equation is given. The natural frequencies and mode shapes of a simply supported beam are obtained for frequencies lower than, equal to and higher than the cut-off frequency. Numerical results are presented for an FGB with the power-law gradient and a laminated beam. The second frequency spectrum is found to exist when frequencies exceed the cut-off frequency. In addition, double frequencies may occur for certain specified geometry of the beam. Previous results for a homogeneous Timoshenko beam can be recovered from the present only letting the material properties be constant. The suggested method is also applicable to layered Timoshenko beams.

1. Introduction

Advanced multilayered composite materials are widely used in many structures of civil, mechanical and space engineering owing to high strength and high stiffness. For instance, a homogeneous elastic layer of ceramic material may be bonded to the surface of a metallic structure and acts as a thermal barrier in a high-temperature environment. However, due to a distinct interface between ceramic and metallic materials, the material properties across the interface undergo a sudden change, which produces stress jump and may further give rise to delamination or cracking of the interface. One way to overcome this shortage is to employ functionally graded materials in which material properties varying continuously, which possess noticeable

E-mail address: xfli@mail.csu.edu.cn

0022-460X/$ - see front matter © 2008 Elsevier Ltd. All rights reserved.
doi:10.1016/j.jsv.2008.04.056

advantages over homogeneous and layered materials in maintaining the integrity of the structure [1]. Such excellent performances allow them to be fabricated as different structures in accordance to various service requirements. To obtain the required optimum performance, the gradient variation of material properties can be achieved by gradually changing the volume fraction of the constituent materials. There are some special manufacturing methods such as high-speed centrifugal casting, powder metallurgy methods, etc to fabricate functionally graded materials [2].

For functionally graded materials, great progress has been made in elasticity theory as well as plates and shells. However, for functionally graded beams (FGB), related studies are very limited. Sankar established a functionally graded Euler–Bernoulli beam model to treat a static problem of a simply supported beam [3]. The corresponding free vibration problem has also been investigated in Ref. [4]. In addition, a new beam finite element has been developed to study the thermoelastic behavior of FGB [5]. Although an FGB with special end conditions may be exactly solved by considering it as an elasticity problem, the calculation involved is fairly cumbersome [6,7]. Therefore, it is necessary to develop a simple beam model which both captures the nature of mechanical behaviors and produces enough accurate results. In the beam theories, the simplest model is the Euler–Bernoulli beam model, in which cross sections perpendicular to the neutral axis prior to bending remain plane and perpendicular to the neutral axis posterior to bending, i.e. the so-called Euler–Bernoulli hypothesis holds. It is well known that the Euler–Bernoulli beam is more suitable for slender beams and lower modes of vibration, and so this theory is inadequate to characterize higher modes of vibration, in particular for short composite beams due to lower shear modulus or shear rigidity. By taking into account the effects of shear deformation, Timoshenko proposed a further improvement of the beam theory [8]. Hitherto, some more accurate models such as higher-order beam theories have been formulated by considering the warping of the cross section. Nevertheless, the Timoshenko beam theory is still widely used owing to its simplicity and efficiency. To date, an efficient generalization of the Timoshenko beam theory to FGB is still lacking, although there are a large number of studies on homogeneous and laminated Timoshenko beams (see e.g. [9–16]). Moreover, it is worth pointing out that in these investigations, usually the free vibration of the Timoshenko and Euler–Bernoulli beams have been studied separately irrespective of use of numerical techniques [9–14] or analytical approaches [15,16].

The objective of this paper is to present a unified approach for analyzing FGB with the rotary inertia and shear deformation included. In Section 2, we establish a single governing equation and derive a general solution of the Timoshenko beam. The Rayleigh and Euler–Bernoulli beams can be analytically reduced from the Timoshenko beam. Section 3 is devoted to a static analysis of a cantilever FGB, where explicit expressions for deflection w and stress distribution are derived. Flexural waves propagating in the FGB are considered in Section 4. Section 5 focuses on the free vibration of an FGB, where the dependence of the natural frequencies and mode shapes on the gradient index for a simply supported beam is given. Finally, numerical results of the natural frequencies of the FGB and layered beams are presented and compared, and conclusions are then drawn.

2. Theoretical model

Consider a beam made of functionally graded materials. Let the beam length be denoted by L, and the cross section be a rectangle of depth h and width b, as shown in Fig. 1. Cartesian coordinates are chosen such that the x-axis is oriented in the axial direction at the midplane of the unbent beam, and the positive z-axis is directed upwards and perpendicular to the x-axis.

Following the treatment of the homogeneous Timoshenko beam theory where the shear deformation and rotary inertia are taken into account simultaneously, the beam deflection $w(x,t)$ and shear deformation $\gamma_{xz}=\gamma(x,t)$ are assumed to be uniform at any cross-sectional area and only dependent on x and t. Consequently, we can express the longitudinal displacement as

$$u(x,z,t)=u_0(x,t)+z\theta, \tag{1}$$

where $u_0(x,t)$ is the longitudinal displacement at the midplane and θ is the rotation of the cross section at the midplane. As a result, the normal strain ε_{xx} and shear strain γ_{xz} can be expressed in terms of u_0, w and θ as

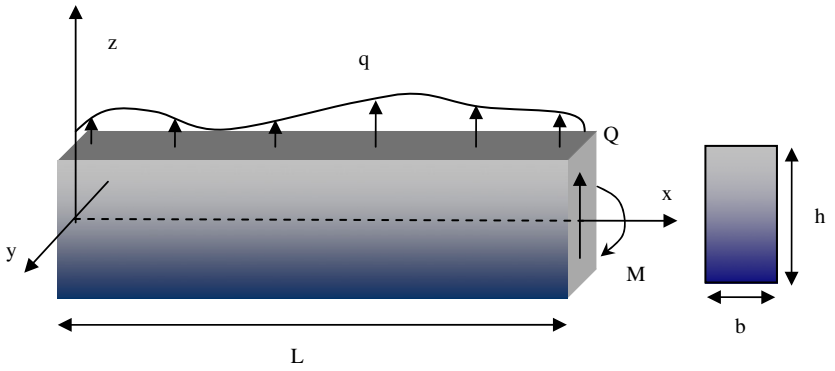

Fig. 1. Schematic of a functionally graded beam and the corresponding coordinates.

follows:

$$\varepsilon_{xx} = \frac{\partial u_0}{\partial x} + z\frac{\partial \theta}{\partial x}, \quad \gamma_{xz} = \theta + \frac{\partial w}{\partial x}. \tag{2}$$

In particular, for shear locking: $\gamma_{xz} = 0$, we have $\theta = -\partial w/\partial x$ and $\varepsilon_{xx} = -z\partial^2 w/\partial x^2$ when $u_0 = 0$, in exact agreement with the well-known result of the Euler–Bernoulli beam theory.

Now we employ the basic differential equations of motion for plane problems

$$\frac{\partial \sigma_{xx}}{\partial x} + \frac{\partial \tau_{xz}}{\partial z} = \rho(z)\frac{\partial^2 u}{\partial t^2}, \tag{3}$$

$$\frac{\partial \tau_{xz}}{\partial x} + \frac{\partial \sigma_{zz}}{\partial z} = \rho(z)\frac{\partial^2 w}{\partial t^2}, \tag{4}$$

where $\rho(z)$ is the depth-dependent mass density of the beam. Using Eq. (1) in Eq. (3) one obtains

$$\frac{\partial \sigma_{xx}}{\partial x} + \frac{\partial \tau_{xz}}{\partial z} = \rho(z)\frac{\partial^2 u_0}{\partial t^2} + z\rho(z)\frac{\partial^2 \theta}{\partial t^2}. \tag{5}$$

Next, straight integration of Eqs. (4) and (5) over the cross-sectional area A gives

$$\frac{\partial Q}{\partial x} + q = \rho_0 \frac{\partial^2 w}{\partial t^2}, \tag{6}$$

$$\frac{\partial N}{\partial x} = \rho_0 \frac{\partial^2 u_0}{\partial t^2} + \rho_1 \frac{\partial^2 \theta}{\partial t^2}, \tag{7}$$

where

$$\rho_j = \int_A z^j \rho(z)\,\mathrm{d}A, \quad j = 0, 1, \ldots, \tag{8}$$

q is the applied prescribed loading per unit length on a lateral surface, the top surface, say, of the beam, and

$$Q = \int_A \tau_{xz}\,\mathrm{d}A, \quad N = \int_A \sigma_{xx}\,\mathrm{d}A. \tag{9}$$

To obtain an equation related to the bending moment M:

$$M = \int_A z\sigma_{xx}\,\mathrm{d}A, \tag{10}$$

one can multiply both sides of Eq. (5) by z and then integrate both sides over the cross-sectional area, yielding

$$\frac{\partial M}{\partial x} - Q = \hat{\rho}_2 \frac{\partial^2 \theta}{\partial t^2}, \tag{11}$$

with the rotary inertia

$$\hat{\rho}_2 = \rho_2 - \frac{\rho_1^2}{\rho_0}, \tag{12}$$

where in deriving the above relation (11) we have used Eq. (7), together with $N = 0$, and the shear-free condition on the top and bottom surfaces of the beam, namely

$$\int_{-h/2}^{h/2} z\frac{\partial \tau_{xz}}{\partial z}\,\mathrm{d}z = z\tau_{xz}|_{z=-h/2}^{z=h/2} - \int_{-h/2}^{h/2} \tau_{xz}\,\mathrm{d}z = -\frac{Q}{b}. \tag{13}$$

As a consequence, we have obtained three equations (6), (7) and (11), describing the functionally graded Timoshenko beam.

Furthermore, with the aid of stress–strain relations for a slender FGB, in the absence of applied axial force N, we finally obtain a pair of coupled governing equations as follows, the detailed process of which is given in Appendix A:

$$G_0^s \frac{\partial}{\partial x}\left(\theta + \frac{\partial w}{\partial x}\right) + q = \rho_0 \frac{\partial^2 w}{\partial t^2}, \tag{14}$$

$$\hat{E}_2 \frac{\partial^2 \theta}{\partial x^2} - G_0^s\left(\theta + \frac{\partial w}{\partial x}\right) = \hat{\rho}_2 \frac{\partial^2 \theta}{\partial t^2}, \tag{15}$$

with

$$\hat{E}_2 = E_2 - \frac{E_1^2}{E_0}. \tag{16}$$

As a check, when the material properties are constants: $E(z) = E, G(z) = G, \rho(z) = \rho$, we have $E_1 = 0, \rho_1 = 0, \rho_2 = \rho I$, I being the inertia of the cross-section area. In this case, the above Eqs. (14) and (15) reduce to

$$G^s A \frac{\partial}{\partial x}\left(\theta + \frac{\partial w}{\partial x}\right) + q = \rho A \frac{\partial^2 w}{\partial t^2}, \tag{17}$$

$$EI \frac{\partial^2 \theta}{\partial x^2} - G^s A\left(\theta + \frac{\partial w}{\partial x}\right) = \rho I \frac{\partial^2 \theta}{\partial t^2}, \tag{18}$$

coinciding with the governing equations for the classical Timoshenko beam theory [8].

Owing to two coupled equations (14) and (15) as well as two unknowns, w and θ, involved, it is desirable to transform them into a single equation with a single unknown, and such a treatment can give rise to great simplification of subsequent calculations. In this aspect, the present method is completely different from previous treatments.

Now by inspection we take

$$w = F - \frac{\hat{E}_2}{G_0^s}\frac{\partial^2 F}{\partial x^2} + \frac{\hat{\rho}_2}{G_0^s}\frac{\partial^2 F}{\partial t^2}, \tag{19}$$

$$\theta = -\frac{\partial F}{\partial x}, \tag{20}$$

where F is a new auxiliary function of length dimension. It is readily checked that Eqs. (14) and (15) are automatically fulfilled only if F satisfies the single fourth-order partial differential equation:

$$\hat{E}_2 \frac{\partial^4 F}{\partial x^4} + \rho_0 \frac{\partial^2 F}{\partial t^2} - \left(\hat{\rho}_2 + \rho_0 \frac{\hat{E}_2}{G_0^s}\right)\frac{\partial^4 F}{\partial x^2 \partial t^2} + \frac{\rho_0 \hat{\rho}_2}{G_0^s}\frac{\partial^4 F}{\partial t^4} = q. \tag{21}$$

Note that the same governing equation for both w and θ similar to Eq. (21) has been derived for the homogeneous Timoshenko beam with a substitution of F by w and θ, respectively (see e.g. Refs. [11,17]). This is not surprising since the nature of the problem does not change, and so the

associated characteristic equation is the same. However, to the best of the author's knowledge, the above governing equation (21) for a single auxiliary function F has never been derived before, even for the homogeneous Timoshenko beam. Its advantage lies in that all physical quantities can be expressed in terms of F and its derivatives, and so boundary conditions associated with discrete restrained ends, including free-end, hinged-end, clamped-end, guided-end, elastically-restrained-end, and so on, are very clear. As seen below, because of such representations, the Rayleigh and Euler–Bernoulli beam theories can be analytically reduced from the Timoshenko beam theory. It is worth noting that although Chervyakov and Nesterenko [18] gave a fourth-order differential equation to describe the Timoshenko beam via using the higher-derivative Lagrangian function and the variational principle, the physical meaning of boundary conditions is not at all obvious and not consistent with those familiar to us, just as pointed out in Ref. [19].

Once F is determined, all the physical quantities of interest are obtainable. For instance, w and θ are given by Eqs. (19) and (20), respectively. In addition, in the absence of applied axial force N, knowledge of Eqs. (A5) and (A9) allows us to represent the bending moment M and shearing force Q in terms of F as follows:

$$M = -\hat{E}_2 \frac{\partial^2 F}{\partial x^2}, \quad Q = -\hat{E}_2 \frac{\partial^3 F}{\partial x^3} + \hat{\rho}_2 \frac{\partial^3 F}{\partial x \partial t^2}. \tag{22}$$

Particularly, the relation $Q = \partial M/\partial x$ holds only the rotary inertia exclusive. With these relations at hand, an alternative pair of relationships of w and θ linking with M reads

$$\frac{\partial^2 w}{\partial x^2} = -\frac{M}{\hat{E}_2} + \frac{M}{G_0^s}\frac{\partial^2 M}{\partial x^2} - \frac{\hat{\rho}_2}{G_0^s \hat{E}_2}\frac{\partial^2 M}{\partial t^2}, \quad \frac{\partial \theta}{\partial x} = \frac{M}{\hat{E}_2}. \tag{23}$$

2.1. Special cases

First, let the rotary inertia be excluded, meaning $\hat{\rho}_2 = 0$. Thus, the final governing equation (21) therefore becomes

$$\hat{E}_2 \frac{\partial^4 F}{\partial x^4} + \rho_0 \frac{\partial^2 F}{\partial t^2} - \rho_0 \frac{\hat{E}_2}{G_0^s}\frac{\partial^4 F}{\partial x^2 \partial t^2} = q, \tag{24}$$

which gives a simplified Timoshenko beam theory. In this case, we have the following representations:

$$w = F - \frac{\hat{E}_2}{G_0^s}\frac{\partial^2 F}{\partial x^2}, \quad \theta = -\frac{\partial F}{\partial x}, \tag{25}$$

$$M = -\hat{E}_2 \frac{\partial^2 F}{\partial x^2}, \quad Q = -\hat{E}_2 \frac{\partial^3 F}{\partial x^3}. \tag{26}$$

Second, consider a special case where $G \to \infty$ or $\kappa \to \infty$, which implies that shear deformation nearly cannot take place, corresponding shear locking $\gamma = 0$. With the requirement, from Eq. (19) we obtain that F is identical to w, and the final governing equation (21) gives

$$\hat{E}_2 \frac{\partial^4 w}{\partial x^4} + \rho_0 \frac{\partial^2 w}{\partial t^2} - \hat{\rho}_2 \frac{\partial^4 w}{\partial x^2 \partial t^2} = q \tag{27}$$

and

$$\theta = -\frac{\partial w}{\partial x}, \quad M = -\hat{E}_2 \frac{\partial^2 w}{\partial x^2}, \quad Q = -\hat{E}_2 \frac{\partial^3 w}{\partial x^3} + \hat{\rho}_2 \frac{\partial^3 w}{\partial x \partial t^2}. \tag{28}$$

Clearly, the above corresponds to the Rayleigh beam theory. Furthermore, if neglecting the effects of the rotary inertia, the above Eq. (27) further simplifies to

$$\hat{E}_2 \frac{\partial^4 w}{\partial x^4} + \rho_0 \frac{\partial^2 w}{\partial t^2} = q, \tag{29}$$

which is the governing equation of the Euler–Bernoulli beam theory.

It is noted that Wang [20] gave an approach for directly obtaining the static bending solution of the homogeneous Timoshenko beam in terms of the bending solution of the Euler–Bernoulli beam. In contrast, here the solutions of the Euler–Bernoulli or Rayleigh beams can be analytically obtained based on the solutions of the Timoshenko beam both for static and dynamic cases, as well as homogeneous and nonhomogeneous cases.

3. Static analysis

From the above, we immediately obtain the static solution of the nonhomogeneous Timoshenko beam. This can be achieved by allowing all time-dependent terms to disappear. Then the governing equation (21) reduces to

$$\hat{E}_2 \frac{d^4 F}{dx^4} = q, \tag{30}$$

which has a solution

$$F = \frac{1}{6\hat{E}_2} \int_0^x q(\xi)(x-\xi)^3 \, \mathrm{d}\xi + C_3 x^3 + C_2 x^2 + C_1 x + C_0, \tag{31}$$

where $C_j (j = 0, 1, 2, 3)$ are constants to be determined through appropriate end conditions.

As an example, consider a cantilever FGB subjected to uniform surface pressure q. Hence, the boundary conditions are

$$M(0) = Q(0) = 0, w(L) = \theta(L) = 0, \tag{32}$$

where the fixed end $x = L$ is assumed. Omitting the detailed procedure, one finally obtains

$$w = q\left[\frac{1}{24\hat{E}_2}(x^4 - 4L^3 x + 3L^4) - \frac{1}{2G_0^s}(x^2 - L^2)\right], \tag{33}$$

$$\sigma_{xx} = \frac{qE(z)}{2\hat{E}_2}\left(z - \frac{E_1}{E_0}\right)x^2. \tag{34}$$

With σ_{xx} at hand, it is easy to obtain shear stress by integrating the equilibrium equation (4) over the cross section

$$\sigma_{xz} = \frac{qx}{\hat{E}_2} \int_{-h/2}^{z} \left(\frac{E_1}{E_0} - z\right) E(z) \, \mathrm{d}z. \tag{35}$$

A comparison of the distribution of stresses σ_{xx} and σ_{xz} between a cantilever FGB and a bi-layered beam, the material properties of which will be given below, is displayed in Figs. 2a,b, respectively.

Obviously, from Fig. 2a, it is seen that σ_{xx} is continuously distributed in a cantilever FGB, while it exhibits an abrupt jump at the interface for a layered beam, as expected. In addition, from Eqs. (34) and (35) the distribution of the normal and shear stresses is seen to be independent of the effective shear modulus, and so their distribution does not change regardless of adopting the Euler–Bernoulli or Timoshenko beam theories. In contrast to the above, the beam deflections are different when adopting the above-mentioned models. In general, the deflection using the Timoshenko beam theory is larger than that using the Euler–Bernoulli beam theory since the latter neglects the contribution of shear deformation towards the deflection. In particular, at the free end the deflection has its maximum as

$$w_{\max} = q\left(\frac{L^4}{8\hat{E}_2} + \frac{L^2}{2G_0^s}\right). \tag{36}$$

For this case with $L/h = 4$, the variation of the ratio of the tip deflections when using the Timoshenko and Euler–Bernoulli beam theories is displayed in Fig. 3. It is seen that the ratios are very close to about 1.063 for either a very large power-law gradient λ (see Eq. (77) below) or a quite small λ. Particularly, this ratio arrives at a minimum 1.055 near $\lambda = 3$. This indicates that the tip deflection of the Euler–Bernoulli beam theory is

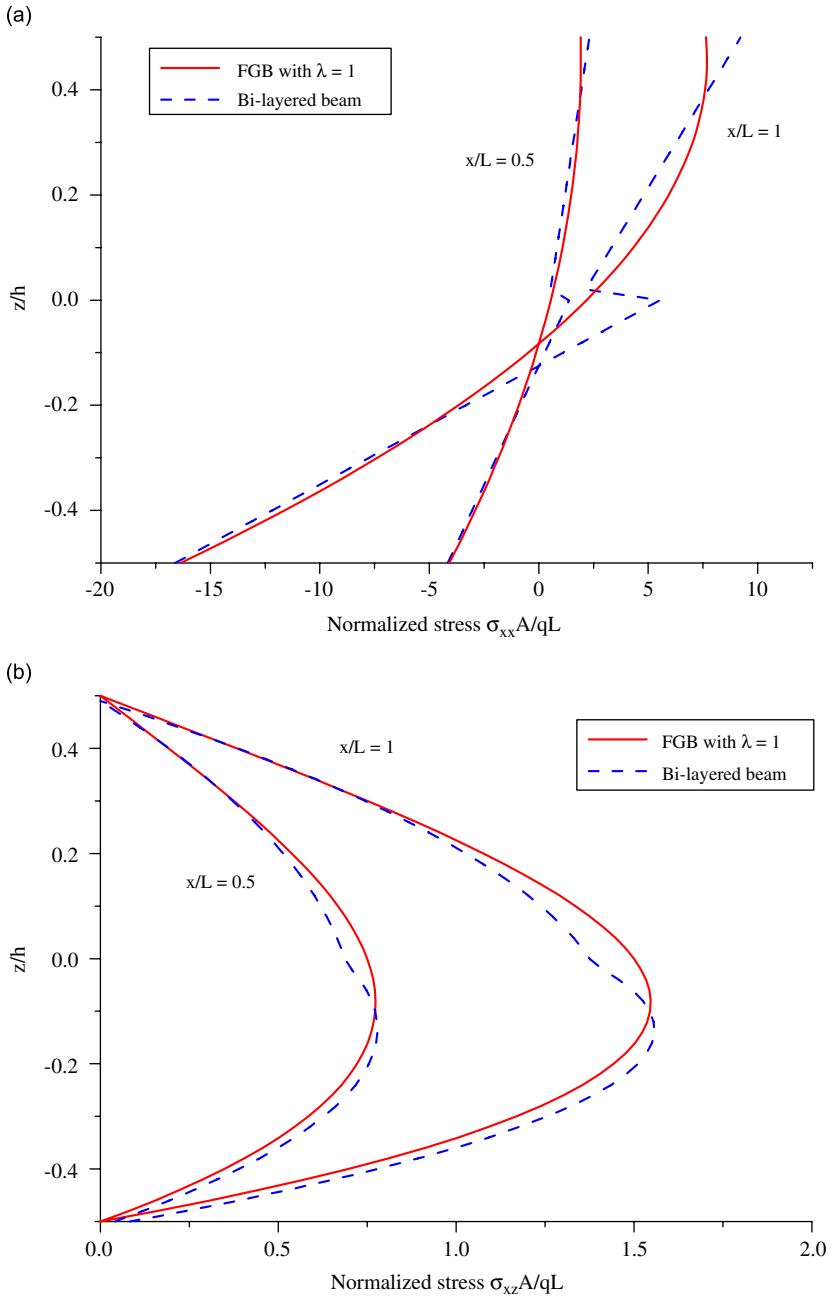

Fig. 2. Comparison of stress distribution in a cantilever FGB, solid lines: FGB with gradient index $\lambda = 1$ in Eq. (77), dashed lines: bi-layered beam with $N = 2$ in Eqs. (78) and (79); (a) dimensionless normal stress $\sigma_{xx}A/qL$, (b) dimensionless shear stress $\sigma_{xz}A/qL$.

underestimated about 6% for $\lambda = 1$ and the length-to-thickness ratio $L/h = 4$. When the beam is homogeneous, the above result (51) collapses to the well-known result. In addition, if the free end of a cantilever beam is subjected to a concentrated force Q, after similar derivations the induced maximum deflection at the free end is

$$w_{\max} = \left(\frac{L^3}{3\hat{E}_2} + \frac{L}{G_0^s}\right) Q. \tag{37}$$

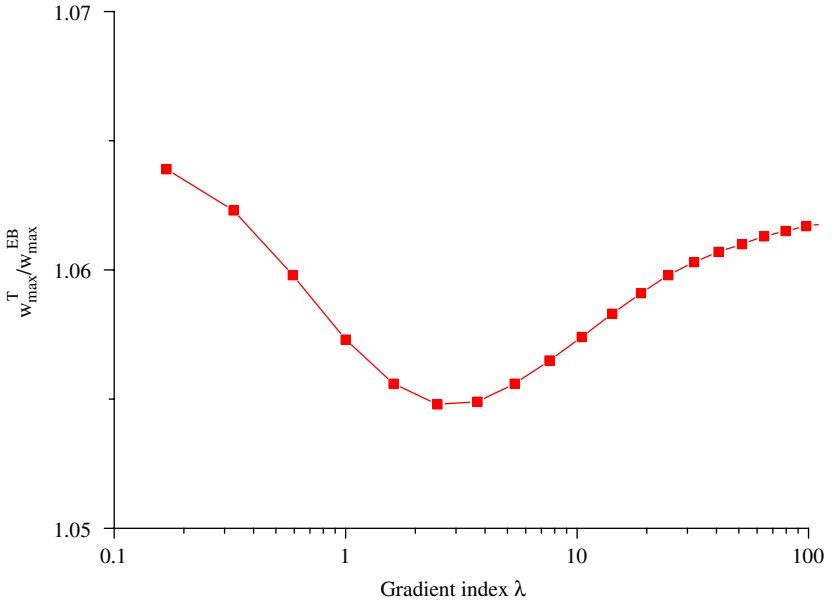

Fig. 3. The ratio of the tip deflection of the FGB using the Timoshenko theory to that using the Euler–Bernoulli theory, w^T_{max}/w^{EB}_{max}, against the gradient index λ.

4. Flexural waves

In this section, let us consider flexural waves propagating in the FGB. For this purpose, the introduced auxiliary function F may take the form

$$F = f(x)e^{i\omega t}, \tag{38}$$

where ω is the frequency. Putting the above into Eq. (21), in the absence of body force and surface pressure, yields

$$\frac{d^4 f}{dx^4} + \left(\frac{\hat{\rho}_2}{\hat{E}_2} + \frac{\rho_0}{G_0^s}\right)\omega^2 \frac{d^2 f}{dx^2} + \left(\frac{\hat{\rho}_2}{G_0^s}\omega^2 - 1\right)\frac{\rho_0}{\hat{E}_2}\omega^2 f = 0, \tag{39}$$

which has the solution

$$f(x) = Ce^{ikx}, \tag{40}$$

where k is the wavenumber. When inserting Eq. (40) back into Eq. (39) one derives the following dispersion equation:

$$\hat{E}_2 k^4 - \left(\hat{\rho}_2 + \rho_0 \frac{\hat{E}_2}{G_0^s}\right)\omega^2 k^2 + \left(\frac{\hat{\rho}_2}{G_0^s}\omega^2 - 1\right)\rho_0 \omega^2 = 0 \tag{41}$$

the solution to which as a quadratic equation in k^2 is easily obtained to be

$$k_1^2 = \frac{\omega^2}{2}\left[\frac{\hat{\rho}_2}{\hat{E}_2} + \frac{\rho_0}{G_0^s} + \sqrt{\left(\frac{\hat{\rho}_2}{\hat{E}_2} - \frac{\rho_0}{G_0^s}\right)^2 + \frac{4\rho_0}{\hat{E}_2\omega^2}}\right], \tag{42}$$

$$k_2^2 = \frac{\omega^2}{2}\left[\frac{\hat{\rho}_2}{\hat{E}_2} + \frac{\rho_0}{G_0^s} - \sqrt{\left(\frac{\hat{\rho}_2}{\hat{E}_2} - \frac{\rho_0}{G_0^s}\right)^2 + \frac{4\rho_0}{\hat{E}_2\omega^2}}\right]. \tag{43}$$

From the above, we make some observations. Recalling $\omega = kv$, v being the wave speed, one obtains only one wave speed:

$$v = \sqrt[4]{\frac{\hat{E}_2}{\rho_0}\omega^2}, \tag{44}$$

for lower frequencies, and two wave speeds:

$$v_1 = \min\left(\sqrt{\frac{\hat{E}_2}{\hat{\rho}_2}}, \sqrt{\frac{G_0^s}{\rho_0}}\right), \quad v_2 = \max\left(\sqrt{\frac{\hat{E}_2}{\hat{\rho}_2}}, \sqrt{\frac{G_0^s}{\rho_0}}\right), \tag{45}$$

for extremely high frequencies. Especially, for the homogeneous Timoshenko beam, the wave speed (44) reduces to

$$v = \sqrt[4]{\frac{EI}{\rho A}\omega^2}, \tag{46}$$

which corresponds to the speed of flexural waves propagating in the Euler–Bernoulli beam, and the latter v_1 and v_2 become, respectively,

$$v_1 = \sqrt{\frac{\kappa G}{\rho}}, \quad v_2 = \sqrt{\frac{E}{\rho}}, \tag{47}$$

corresponding to two speeds of flexural waves propagating in the Timoshenko beam for extremely high frequencies [21].

For general frequencies, from Eqs. (42) and (43), there is only one wave speed:

$$v_1 = \sqrt{\frac{2}{\dfrac{\hat{\rho}_2}{\hat{E}_2} + \dfrac{\rho_0}{G_0^s} + \sqrt{\left(\dfrac{\hat{\rho}_2}{\hat{E}_2} + \dfrac{\rho_0}{G_0^s}\right)^2 + \dfrac{4\rho_0}{\hat{E}_2}\left(\dfrac{1}{\omega^2} - \dfrac{1}{\omega_c^2}\right)}}}, \tag{48}$$

when frequencies are lower than the cut-off frequency or critical frequency: $\omega_c = \sqrt{G_0^s/\hat{\rho}_2}$. However, when frequencies exceed ω_c, there are two branches of flexural wave with speeds v_1, still given by Eq. (48), and v_2:

$$v_2 = \sqrt{\frac{2}{\dfrac{\hat{\rho}_2}{\hat{E}_2} + \dfrac{\rho_0}{G_0^s} - \sqrt{\left(\dfrac{\hat{\rho}_2}{\hat{E}_2} + \dfrac{\rho_0}{G_0^s}\right)^2 + \dfrac{4\rho_0}{\hat{E}_2}\left(\dfrac{1}{\omega^2} - \dfrac{1}{\omega_c^2}\right)}}}. \tag{49}$$

For the case of $\omega = \omega_c$, it is readily found that in this case wave propagates with a constant velocity $v = ((\hat{\rho}_2/\hat{E}_2) + (\rho_0/G_0^s))^{-1/2}$ in the Timoshenko beam.

In particular, if the effect of the rotary inertia is disregarded, the higher branch disappears and the lower branch reduces to

$$v_1 = \sqrt{\frac{2}{\dfrac{\rho_0}{G_0^s} + \sqrt{\left(\dfrac{\rho_0}{G_0^s}\right)^2 + \dfrac{4\rho_0}{\hat{E}_2\omega^2}}}}, \tag{50}$$

whereas if shear locking is taken into account, the higher branch also disappears and the lower branch is given by

$$v_1 = \sqrt{\frac{2}{\dfrac{\hat{\rho}_2}{\hat{E}_2} + \sqrt{\left(\dfrac{\hat{\rho}_2}{\hat{E}_2}\right)^2 + \dfrac{4\rho_0}{\hat{E}_2\omega^2}}}}. \tag{51}$$

Furthermore, when the influences of shear deformation and rotary inertia are simultaneously ignored, Eqs. (50) and (51) give only one wave speed (44) for lower frequencies, as expected. In effect, the wave speed given by Eq. (44) corresponds to the velocity of flexural waves propagating in the functionally graded Euler–Bernoulli beam.

5. Free vibration

Here we analyze free vibration of the FGB. With the results derived in the foregoing section, one can write a general solution to Eq. (39) as

$$f(x) = C_1 \cos \alpha x + C_2 \sin \alpha x + C_3 \cosh \beta x + C_4 \sinh \beta x \tag{52}$$

for lower frequencies $\omega < \omega_c$ (Case A),

$$f(x) = C_1 \cos \alpha x + C_2 \sin \alpha x + C_3 \cos \beta x + C_4 \sin \beta x \tag{53}$$

for higher frequencies $\omega > \omega_c$ (Case B), and

$$f(x) = C_1 \cos\left(x\sqrt{\frac{G_0^s}{\hat{E}_2} + \frac{\rho_0}{\hat{\rho}_2}}\right) + C_2 \sin\left(x\sqrt{\frac{G_0^s}{\hat{E}_2} + \frac{\rho_0}{\hat{\rho}_2}}\right) + C_3 + C_4 x, \tag{54}$$

for $\omega = \omega_c$ (Case C), respectively, where

$$\alpha = \omega\sqrt{\frac{1}{2}\left[\sqrt{\left(\frac{\hat{\rho}_2}{\hat{E}_2} - \frac{\rho_0}{G_0^s}\right)^2 + \frac{4\rho_0}{\hat{E}_2\omega^2}} + \left(\frac{\hat{\rho}_2}{\hat{E}_2} + \frac{\rho_0}{G_0^s}\right)\right]}, \tag{55}$$

$$\beta = \omega\sqrt{\pm\frac{1}{2}\left[\sqrt{\left(\frac{\hat{\rho}_2}{\hat{E}_2} - \frac{\rho_0}{G_0^s}\right)^2 + \frac{4\rho_0}{\hat{E}_2\omega^2}} - \left(\frac{\hat{\rho}_2}{\hat{E}_2} + \frac{\rho_0}{G_0^s}\right)\right]}, \tag{56}$$

and the sign $\pm$ in Eq. (56) corresponds to $\omega < \omega_c$ (upper) and $\omega > \omega_c$ (lower), respectively. It is especially noted that the sine and cosine terms in Eqs. (52)–(54) correspond to waves propagating in the FGB, while other terms represent nonpropagating fields or evanescent components [22]. Furthermore, if neglecting the effects of either shear deformation or the rotary inertia, meaning $\omega_c \to \infty$, the general solutions (53) and (54) cannot occur. In other words, shear deformation-dominated or rotation-dominated vibrations at higher frequencies are discarded. For the homogeneous Timoshenko beam, the spectrum characteristic and physical interpretations reflected from the general solution (53) have been elucidated in Refs. [23,24].

With these formulae at hand, natural frequencies for some typical situations can be easily determined. As an example, consider a simply supported FGB, and the corresponding boundary conditions read

$$w(0) = M(0) = 0, \quad w(L) = M(L) = 0. \tag{57}$$

For case A, with the solution (52) and using Eq. (19), the deflection and bending moment are expressed by

$$w = C_1\eta_1 \cos \alpha x + C_2\eta_1 \sin \alpha x + C_3\eta_2 \cosh \beta x + C_4\eta_2 \sinh \beta x, \tag{58}$$

$$M = \hat{E}_2(C_1\alpha^2 \cos \alpha x + C_2\alpha^2 \sin \alpha x - C_3\beta^2 \cosh \beta x - C_4\beta^2 \sinh \beta x) \tag{59}$$

where

$$\eta_1 = 1 + \frac{\hat{E}_2}{G_0^s}\alpha^2 - \frac{\hat{\rho}_2}{G_0^s}\omega^2, \quad \eta_2 = 1 - \frac{\hat{E}_2}{G_0^s}\beta^2 - \frac{\hat{\rho}_2}{G_0^s}\omega^2. \tag{60}$$

Consequently, the boundary conditions (57) are transformed to the following set:

$$D[C_1, C_2, C_3, C_4]^{\mathrm{T}} = 0, \tag{61}$$

where the superscript T denotes the transpose of a matrix, and

$$D=\begin{bmatrix} \eta_1 & 0 & \eta_2 & 0 \\ \alpha^2 & 0 & -\beta^2 & 0 \\ \eta_1\cos\alpha L & \eta_1\sin\alpha L & \eta_2\cosh\beta L & \eta_2\sinh\beta L \\ \alpha^2\cos\alpha L & \alpha^2\sin\alpha L & -\beta^2\cosh\beta L & -\beta^2\sinh\beta L \end{bmatrix}. \tag{62}$$

Since this set has a nontrivial solution, the determinant of the coefficient of this set must disappear, namely

$$\det D=0. \tag{63}$$

Solving Eq. (63) results in $\sin\alpha L=0$, and we have $\alpha_n=n\pi/L(n=1,2,\ldots)$, which in turn is inserted back into Eq. (55), yielding the natural frequencies of the simply supported FGB:

$$\omega_n^2=\frac{2\hat{E}_2\alpha_n^4}{\rho_0}\frac{1}{\zeta_n+\sqrt{\zeta_n^2-\dfrac{4\hat{\rho}_2\hat{E}_2}{\rho_0 G_0^s}\alpha_n^4}}, \tag{64}$$

$$\zeta_n=1+\alpha_n^2\left(\frac{\hat{\rho}_2}{\rho_0}+\frac{\hat{E}_2}{G_0^s}\right). \tag{65}$$

Clearly, without the rotary inertia, meaning $\hat{\rho}_2=0$, the natural frequencies (64) become

$$\omega_n=\alpha_n^2\sqrt{\frac{\hat{E}_2}{\rho_0}\frac{G_0^s}{G_0^s+\hat{E}_2\alpha_n^2}}. \tag{66}$$

On the other hand, if considering the shear locking in Eq. (64), the natural frequencies are

$$\omega_n=\alpha_n^2\sqrt{\frac{\hat{E}_2}{\rho_0+\hat{\rho}_2\alpha_n^2}}. \tag{67}$$

Furthermore, if both the rotary inertia and the shear deformation are excluded, we obtain

$$\omega_n=\alpha_n^2\sqrt{\frac{\hat{E}_2}{\rho_0}}, \tag{68}$$

which, when material properties are constants, gives

$$\omega_n=\left(\frac{n\pi}{L}\right)^2\sqrt{\frac{EI}{\rho A}}, \tag{69}$$

in exact agreement with the well-known natural frequencies for the simply supported Euler–Bernoulli beam.

For case B: $\omega>\omega_c$, a procedure similar to the above can lead to the following results $\sin\alpha L\sin\beta L=0$, which gives

$$\alpha_n=\frac{n\pi}{L},\ \text{or}\ \beta_n=\frac{n\pi}{L},\quad n=1,2,\ldots \tag{70}$$

Therefore, we conclude that the natural frequencies corresponding to α_n are still given by (64), while those corresponding to β_n are analogously derived from Eq. (56) as

$$\omega_n^2=\frac{2\hat{E}_2\beta_n^4}{\rho_0}\frac{1}{\zeta_n-\sqrt{\zeta_n^2-\dfrac{4\hat{\rho}_2\hat{E}_2}{\rho_0 G_0^s}\beta_n^4}}. \tag{71}$$

Then, apart from Eq. (64) there are other natural frequencies given by Eq. (71). When studying free vibration of the homogeneous Timoshenko beam and shear beam, some researchers refer to such a phenomenon as

double eigenvalues or double frequencies [25–27]. For subsequent convenience, two frequencies given by Eqs. (64) and (71) for a given n are referred to as the first and second spectra, respectively. For such double frequencies, it is not difficult to show the mode shapes of vibration corresponding to Eqs. (64) and (71) to be

$$w_n = \frac{1}{2}\left[1 + \alpha_n^2\left(\frac{\hat{E}_2}{G_0^s} - \frac{\hat{\rho}_2}{\rho_0}\right) \pm \sqrt{\zeta_n^2 - \frac{4\hat{\rho}_2\hat{E}_2}{\rho_0 G_0^s}\alpha_n^4}\right]\sin\alpha_n x, \tag{72}$$

$$\theta_n = -\alpha_n \cos\alpha_n x, \tag{73}$$

where the signs $\pm$ correspond to the first and second spectra, respectively. Obviously, the first vibrational mode gives a larger amplitude, while the second gives a smaller amplitude. From this point, one may say that mode shapes of vibration show apparent discrepancy. However, two vibration modes give the same rotation.

For case C, free vibration of a simply supported FGB cannot occur unless $L/\pi\sqrt{(\hat{\rho}_2/\hat{E}_2) + (\rho_0/G_0^s)}$ is a certain positive integer, i.e. $L/\pi\sqrt{(\hat{\rho}_2/\hat{E}_2) + (\rho_0/G_0^s)} = n$. Denoting $\alpha_n = n\pi/L$ as well, this case gives its unique vibrational mode as

$$w_n = \frac{\hat{E}_2}{G_0^s}\alpha_n^2 \sin\alpha_n x, \quad \theta_n = -\alpha_n \cos\alpha_n x. \tag{74}$$

6. Numerical results

In this section, several numerical results are presented and a comparison of wave speeds as well as natural frequencies is made. In the following computation we take the length $L = 0.5\,\mathrm{m}$, depth $h = 0.125\,\mathrm{m}$ and shear correction factor $\kappa = 5(1+\nu)/(6+5\nu)$. In practice, Poisson's ratio commonly varies slightly, and so we take $\nu = 0.3$ hereafter, although depth-dependent Poisson's ratio $\nu(z)$ can be treated similarly, and does not create any difficulty. Assume that the beam is a mixture of two materials, Steel and Aluminum, and relevant material properties are, respectively,

$$E_{\mathrm{Steel}} = 210\,\mathrm{GPa}, \rho_{\mathrm{Steel}} = 7850\,\mathrm{kg/m^3}, \tag{75}$$

$$E_{\mathrm{Al}} = 70\,\mathrm{GPa}, \rho_{\mathrm{Al}} = 2707\,\mathrm{kg/m^3}. \tag{76}$$

Based on the present method, the gradient variation may be chosen arbitrarily, although it is commonly assumed to show exponential-type dependence for the sake of simplicity of mathematical treatment [28]. However, from an experimental view, it is constructive to adopt a power-law gradient [29]. In this case, the effective material properties of the beam are governed by

$$E(z) = E_b + (E_t - E_b)\left(\frac{z}{h} + \frac{1}{2}\right)^{\lambda}, \quad \rho(z) = \rho_b + (\rho_t - \rho_b)\left(\frac{z}{h} + \frac{1}{2}\right)^{\lambda}, \tag{77}$$

where λ is a non-negative constant describing the volume fraction, which can be determined by experimental data. Here a variable with the subscripts b or t specifies the one at the bottom or the top surface of the beam. From these relations, when $z = -h/2, E = E_b, \rho = \rho_b$; and when $z = h/2$, $E = E_t, \rho = \rho_t$. For simplicity, let the bottom surface be steel rich, and the top surface be aluminum rich, respectively. It is wellknown that such a power-law relation is not exact and many more accurate approximations may be found. However, the above power-law relation is easily dominated via variations of the volume fraction of steel and aluminum from the bottom to the top in experiment [30].

Firstly, wave speeds when using various beam theories are calculated and displayed in Fig. 4, where solid lines correspond to the results of FGB, and dashed lines to those of a bi-layered beam. Obviously, the wave speed when neglecting the rotary inertia is quite close to that for the lower branch using the Timoshenko beam theory, whereas the wave speed in the case of shear locking gradually tends to that of the higher branch for extremely high frequencies. When frequencies are lower, the wave speed for the Euler–Bernoulli beam gives a good approximation of the first branch wave speed for the Timoshenko beam. However, with an increase in

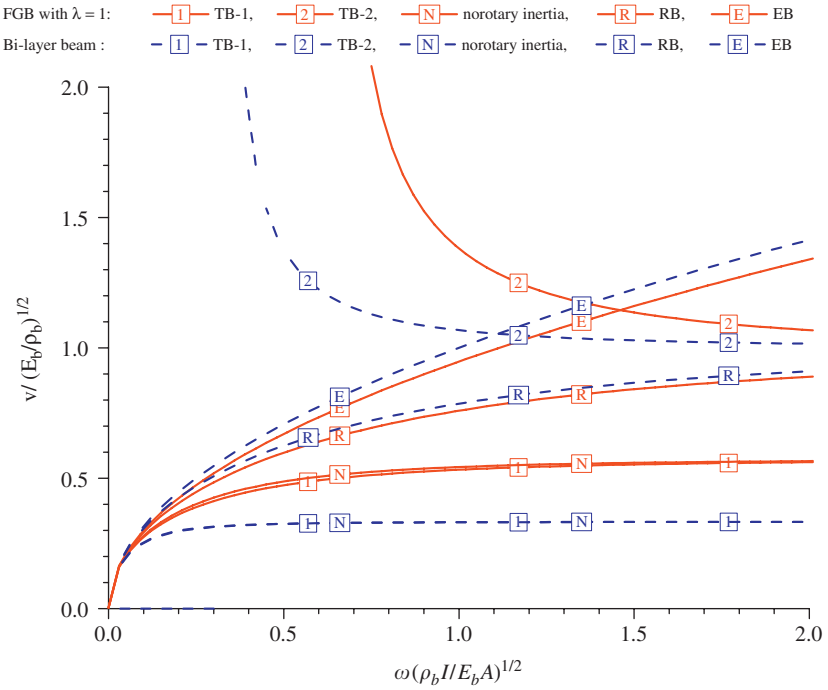

Fig. 4. Normalized wave speeds, $v/\sqrt{E_b/\rho_b}$, against frequencies, solid lines: FGB, dashed lines: bi-layered beam, TB: Timoshenko beam, RB: Rayleigh beam, EB: Euler–Bernoulli beam.

frequencies, the former is deviated away from the latter, implying that it is not adequate to use the Euler–Bernoulli beam theory for high frequencies. Also, the wave speed of the higher branch does not occur unless frequencies exceed the cut-off frequency. On the other hand, compared to the wave speeds of a bi-layered beam, the consideration of gradient variation in the thickness increases the wave speeds and cut-off frequency for the Timoshenko beam with and without the effects of the rotary inertia, but slightly decreases the wave speed for the Rayleigh and Euler–Bernoulli beams. This indicates that when gradient variation is taken into account, the influence of the shear deformation is more significant than that of the rotary inertia.

Next, as a check, we consider a homogeneous Timoshenko beam with simply supported ends, and the first 15 natural frequencies of steel and aluminum are tabulated in Table 1, where the data with asterisk are evaluated from the second spectrum (71). One finds that for the steel beam the obtained results corresponding to the first spectrum (64) are identical to those derived in Ref. [19]. If using $\kappa = 5/6$ instead of $\kappa = 5(1+\nu)/(6+5\nu)$, a direct computation indicates that our results, which are not listed in Table 1, are in exact agreement with those given in Ref. [23]. It is concluded that the above-proposed method is efficient and accurate.

Furthermore, we examine the natural frequencies of a simply supported FGB. The first 15 natural frequencies for the FGB with gradient index $\lambda = 1$ are tabulated in Table 2. For comparison, we consider multilayered beams. In each layer, all material properties are chosen to be constants, i.e.

$$E(z) = E_b + (E_t - E_b)\frac{i-1}{N-1}, \quad \frac{i-1}{N} \leqslant \frac{z}{h} + \frac{1}{2} < \frac{i}{N}, \tag{78}$$

$$\rho(z) = \rho_b + (\rho_t - \rho_b)\frac{i-1}{N-1}, \quad \frac{i-1}{N} \leqslant \frac{z}{h} + \frac{1}{2} < \frac{i}{N}, \tag{79}$$

where $i(1 \leqslant i \leqslant N)$ denotes the ith layer and N is the number of layers $(N > 1)$. Using the above-established formulae, the natural frequencies of this case can be evaluated and the obtained results are also listed in Table 2. From this table, one easily observes that natural frequencies of laminated beams approach those of FGB with

Table 1
The first 15 natural frequencies (rad/s) for homogeneous Timoshenko beams

n	Steel	Al
1	6728.89	6615.66
2	22279.03	21904.14
3	41094.04	40402.57
4	60889.98	59865.40
5	80895.78	79534.57
CF	82755.11	81362.61
6	90616.10*	89091.33*
7	100855.65	99158.58
8	109474.39*	107632.30*
9	120693.16	118662.29
10	133540.31*	131293.26
11	140396.00	138033.60
12	159973.97	157282.14
13	160222.27*	157526.26*
14	179443.08	176423.64
15	188435.57*	185264.82

Frequencies marked with asterisk are evaluated from Eq. (71), others from Eq. (64), and CF is the cut-off frequency.

Table 2
The first 15 natural frequencies (rad/s) for nonhomogeneous Timoshenko beams

Mode number	Laminated beam						FGM beam
	2 layers	5 layers	10 layers	20 layers	50 layers	100 layers	$\lambda = 1$
1	6132.11	6346.33	6405.12	6432.24	6447.83	6453.11	6457.93
2	20796.52	21330.23	21474.46	21540.65	21578.62	21591.46	21603.18
3	39046.39	39776.87	39972.04	40061.29	40112.40	40129.67	40145.42
4	58549.54	59369.36	59586.63	59685.73	59742.41	59761.55	59779.01
5	78422.46	79267.14	79489.65	79590.93	79648.81	79668.35	79686.16
CF	90884.98	87537.74	86651.98	86247.16	86016.01	85937.9	85866.71
6	98012.60*	94928.87*	94115.53*	93744.10*	93532.16*	93460.56*	93395.31*
7	98335.06	99169.32	99388.04	99487.45	99544.22	99563.38	99580.84
8	115600.86*	112975.74*	112286.18*	111971.43*	111792.03*	111731.43*	111676.22*
9	118167.93	118973.69	119184.15	119279.69	119334.22	119352.62	119369.38
10	137884.80	136311.59*	135729.66*	135463.94*	135312.67*	135261.57*	135215.02*
11	138533.03*	138653.78	138854.03	138944.85	138996.66	139014.14	139030.07
12	157482.45	158211.78	158401.24	158487.11	158536.08	158552.60	158567.64
13	164243.50*	162359.79*	161867.51*	161642.50*	161514.60*	161471.38*	161432.03*
14	176970.03	177659.77	177838.60	177919.59	177965.78	177981.35	177995.54
15	191598.11*	190006.15*	189591.11*	189401.11*	189293.31*	189256.87*	189223.70*

Frequencies marked with asterisk are evaluated from Eq. (71), others from Eq. (64), and CF is the cut-off frequency.

the number of layer N increasing, as expected. However, when $N = 100$, there is still a slight difference between the obtained results of FGB and laminated beams.

The influence of the gradient index λ on dimensionless natural frequencies, $\Omega_n = \omega_n L/\sqrt{E_b/\rho_b}$, is shown in Figs. 5a,b for the first two natural frequencies of the first and second spectra, respectively. As seen in Fig. 5a, the dimensionless natural frequencies Ω_n related to Eq. (64) decrease with increasing λ, arriving at its minimum at a certain λ value, and increase as λ continues to rise. Such a trend is reversed for the dimensionless natural frequencies Ω_n corresponding to Eq. (71). These results coincide with those presented in Table 2, from which one can find that when the number of layers rises, the data without asterisk associated with the first spectrum are increased, while those with asterisk associated with the second spectrum are decreased. This phenomenon

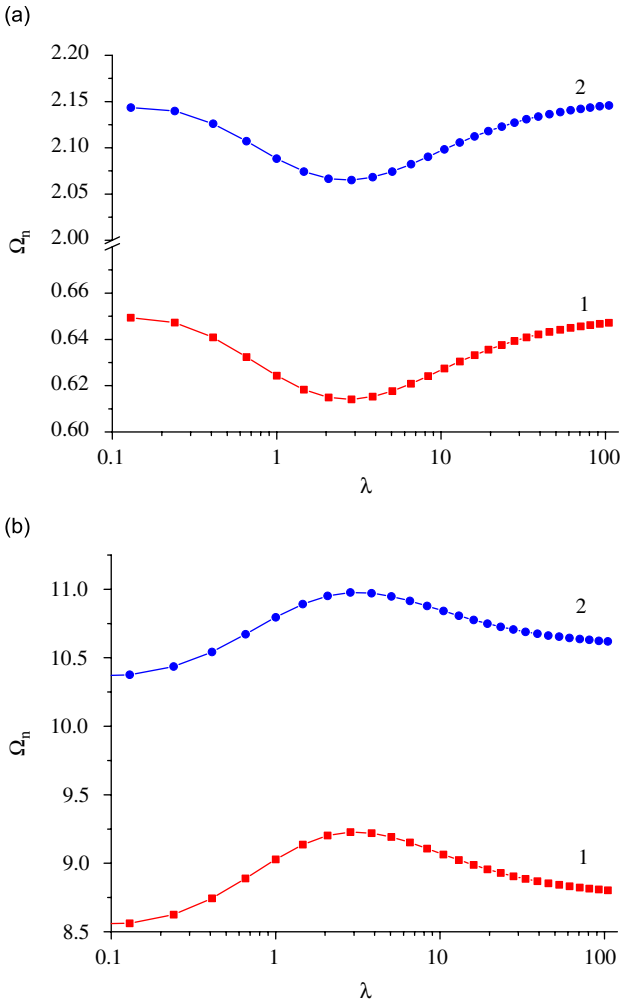

Fig. 5. Dimensionless natural frequencies $\Omega_n = \omega_n L/\sqrt{E_b/\rho_b}$ versus the gradient index λ, (a) the first frequency spectrum associated with Eq. (64), (b) the second frequency spectrum associated with Eq. (71).

is different from that observed in Ref. [7]. The reason is due to the different material properties used. Therefore, material properties play a dominant role in determining natural frequencies, even for the same gradient variation. In other words, natural frequencies are sensitive to the constituents of each phase. Additionally, only the first four vibrational modes are plotted in Ref. [7]. In general, the natural frequencies dominated by the second spectrum correspond to higher vibrational modes, e.g. the nth ($n \geqslant 6$) modes in Table 2.

To show the existence of the double frequencies for the homogeneous and nonhomogeneous beams with simply supported ends, Fig. 6 displays the variation of dimensionless natural frequencies against the ratio of the gyration radius-to-span for the homogeneous Timoshenko beam. In this figure, only the first six frequencies of the first spectrum (64) and the first three frequencies of the second spectrum (71) are plotted, and it is found that at certain values of r_g/L, r_g being the gyration radius $\sqrt{I/A}$, the frequency curves corresponding to Eq. (71) cross the frequency curves corresponding to Eq. (64), and the frequencies at the intersecting position manifest the existence of double frequencies. For example, at about $r_g/L = 0.1062$, the fourth-mode frequency given by the first spectrum (64) is about 6.3676, identical to the first-mode frequency by the second spectrum (71). It is especially emphasized that when two curves go through the double frequencies, the lower and higher frequency branches interchange. For example, the fourth natural frequency corresponds to A_1A_2 (see Fig. 6) given by Eq. (64) with $n = 4$, after crossing double frequency point A_2 it

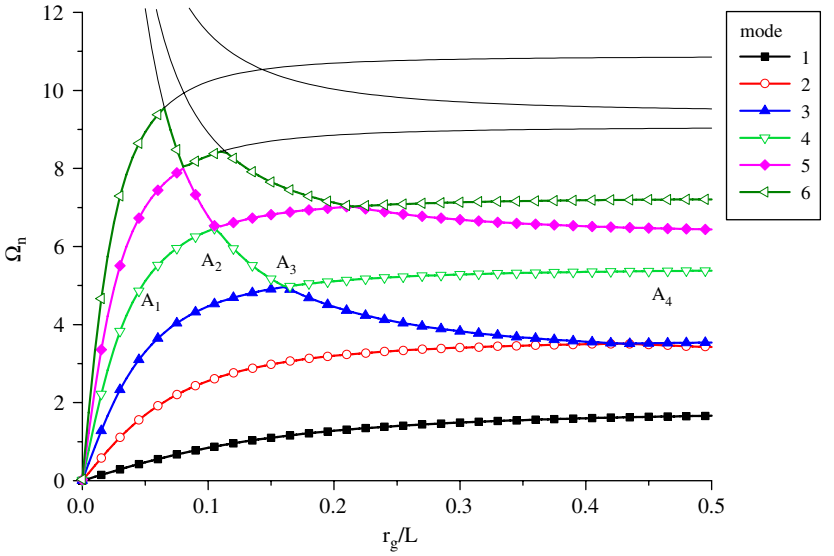

Fig. 6. Dimensionless natural frequencies $\Omega_n = \omega_n L/\sqrt{E_b/\rho_b}$ as a function of the gyration radius-to-span ratio r_g/L for the first and second frequency spectra.

Table 3
r_g/L values for the occurrence of double frequencies between the first and second frequency spectra

(n,m)	λ					
	0	0.1	0.5	1	2	10
(2, 1)	0.4292	0.4240	0.4334	0.4446	0.4534	0.4467
(3, 1)	0.1612	0.1591	0.1634	0.1679	0.1712	0.1681
(4, 1)	0.1062	0.1048	0.1077	0.1107	0.1129	0.1108
(5, 1)	0.0805	0.0794	0.0816	0.0839	0.0855	0.0840
(4, 2)	0.2146	0.2120	0.2167	0.2223	0.2267	0.2234
(5, 2)	0.1128	0.1114	0.1143	0.1174	0.1197	0.1177

drops along the curve A_2A_3 corresponding to the first natural frequency evaluated by Eq. (71) with $n = 1$, and finally crossing double frequency point A_3 it grows gradually along A_3A_4 corresponding to the third natural frequency of Eq. (64) with $n = 3$. That is, the down triangle curve forms the fourth-mode natural frequency curve. If double frequencies occur for certain r_g/L, then the smaller the r_g/L, the higher the double frequencies become. Note that with increasing r_g/L, the frequency curves evaluated from Eq. (71) decrease, while those from Eq. (64) increase. Consequently, the double frequency phenomenon cannot take place when disregarding the effects of the rotary inertia and shear deformation. A similar phenomenon can be observed for the FGB. The r_g/L values corresponding to the positions of the double frequencies appearing are dependent on the gradient index λ, which are listed in Table 3 for $r_g/L<0.4$, and $m,n<6$. In this table, n and m denote the corresponding modal numbers of the first and second frequency spectra, respectively.

In addition, besides the natural frequencies corresponding to Eq. (71), an intersection between the cut-off frequency curve and the first frequency-spectrum curves takes place for certain specified geometry of the beam. This can be seen in Fig. 7 for the homogeneous Timoshenko beam. In Fig. 7, the numerals denote the number of the corresponding vibrational modes. Clearly the number of vibrational modes changes when crossing points at which double frequencies occur. This indicates that double frequencies widely exist not only between the first frequency spectrum and the second frequency spectrum but also between the first frequency spectrum and the critical frequency. The latter has not been studied before, even for the homogeneous beam. The dependence of the double frequencies on r_g/L for various gradient indexes is given in Table 4.

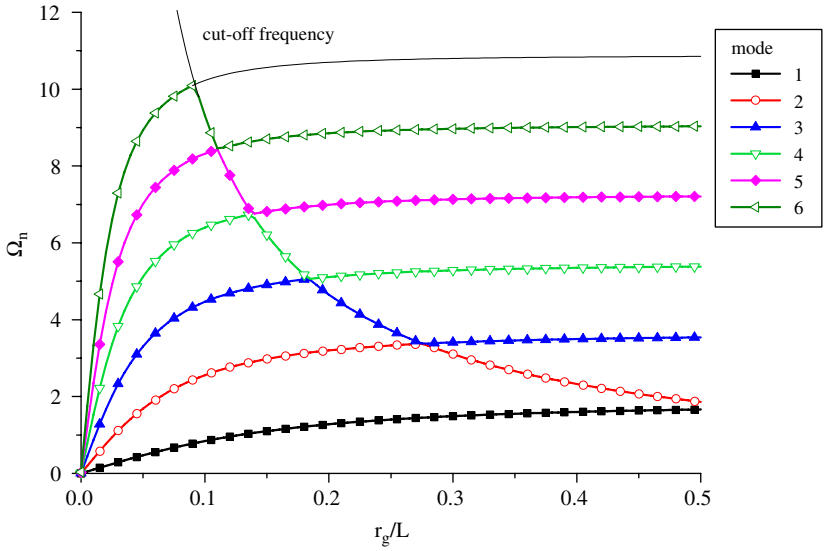

Fig. 7. Dimensionless natural frequencies $\Omega_n = \omega_n L/\sqrt{E_b/\rho_b}$ as a function of the gyration radius-to-span ratio r_g/L for the first frequency spectrum and cut-off frequency.

Table 4
r_g/L values for the occurrence of double frequencies between the first frequency spectrum and cut-off frequency

n	λ					
	0	0.1	0.5	1	2	10
2	0.2759	0.2724	0.2799	0.2876	0.2933	0.2879
3	0.1839	0.1816	0.1866	0.1917	0.1955	0.1919
4	0.1380	0.1362	0.1400	0.1438	0.1466	0.1440
5	0.1104	0.1090	0.1120	0.1150	0.1173	0.1152

Finally, the mode shapes of vibration of the FGB with gradient index $\lambda = 1$ are shown in Fig. 8 for the first three natural frequencies of the first and second frequency spectra, respectively. From Fig. 8, it can be found that for $h/L = 0.1$, the mode shapes related to the second frequency spectrum become negligible as compared to those of its counterpart for the first frequency spectrum. Moreover, for small h/L values, the mode shapes of vibration are very close to those for the Euler–Bernoulli beam, which are plotted by gray thick curves in Fig. 8. When the ratio h/L becomes large, e.g. $h/L = 0.25$, the effects of shear deformation in Timoshenko beams become remarkable. In addition, the mode shapes of vibration corresponding to the second frequency spectrum are seen to be always opposite to those for the first frequency spectrum, and the corresponding amplitudes are smaller.

7. Conclusions

The Timoshenko beam theory is extended to treat FGB as well as layered beams. Different from previous approaches, a single fourth-order partial differential equation has been derived. All physical quantities of interest can be expressed in terms of the solution of the resulting equation. A static result is presented for a cantilever FGB. Also, a dynamic analysis including wave propagation and free vibration is performed. Two wave speeds are obtained when using the Timoshenko beam theory, and the higher branch disappears for frequencies lower than the cut-off frequency. Furthermore, free vibration of a nonhomogeneous beam is considered. The natural frequencies and mode shapes for a simply supported beam are given for frequencies

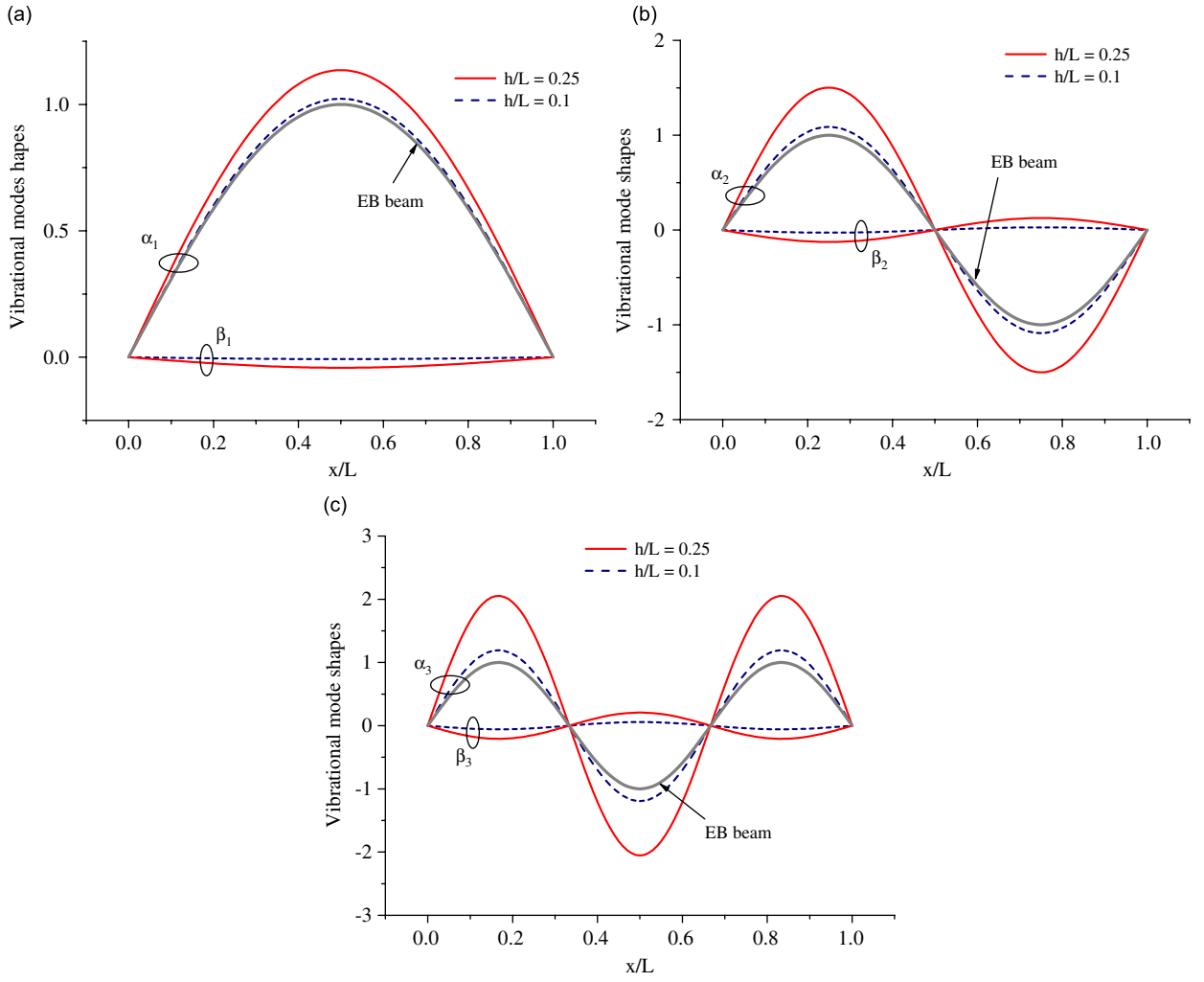

Fig. 8. The first three mode shapes of vibration: (a) the first mode, (b) the second mode, (c) the third mode.

lower than, equal to and higher than the cut-off frequency. Numerical results are presented for an FGB of a power-law gradient and a multilayered beam. The second frequency spectrum is found to exist when frequencies exceed the cut-off frequency. In addition, double frequencies may occur at certain specified geometry of the beam. When the effects of the rotary inertia and shear deformation are neglected simultaneously, the present results reduce to those of the functionally graded Euler–Bernoulli beam.

Acknowledgments

This work was supported by the National Natural Science Foundation of China under Grant No. 10672189. The author would like to thank three anonymous reviewers for giving helpful suggestions to improve the original manuscript.

Appendix A

In order to obtain governing equations for the functionally graded Timoshenko beam, it is necessary to derive relationships of the bending moment M, shearing force Q and axial force N with the deflection w,

rotation θ and displacement u_0. To this end, using the stress–strain relations for a slender beam

$$\sigma_{xx} = E(z)\varepsilon_{xx}, \quad \tau_{xz} = G^s(z)\gamma_{xz}, \tag{A.1}$$

where $G^s(z) = \kappa G(z)$ stands for the reduced shear modulus, κ being the shear correction factor, which is introduced to account for the relaxation of the inconsistency of the usual shear-free boundary condition at the beam surface [8]. $E(z)$ and $v(z)$ are the depth-dependent Young's modulus and Poisson's ratio of the beam.

Substituting Eq. (2) into Eq. (A.1) yields

$$\sigma_{xx} = E(z)\left(\frac{\partial u_0}{\partial x} + z\frac{\partial \theta}{\partial x}\right), \tag{A.2}$$

$$\tau_{xz} = G^s(z)\left(\theta + \frac{\partial w}{\partial x}\right). \tag{A.3}$$

Upon performing integration at both sides of Eqs. (A.2) and (A.3) over the cross-sectional area, the axial force N and shearing force Q can be expressed below

$$N = E_0\frac{\partial u_0}{\partial x} + E_1\frac{\partial \theta}{\partial x}, \tag{A.4}$$

$$Q = G_0^s\left(\theta + \frac{\partial w}{\partial x}\right), \tag{A.5}$$

with

$$E_j = \int_A s^j E(s)\,\mathrm{d}A, \quad G_j^s = \int_A s^j G^s(s)\,\mathrm{d}A. \tag{A.6}$$

Furthermore, we multiply both sides of Eq. (A.2) by z and then integrate over the cross-sectional area, leading to

$$M = E_1\frac{\partial u_0}{\partial x} + E_2\frac{\partial \theta}{\partial x}. \tag{A.7}$$

Eliminating $\partial u_0/\partial x$ from Eqs. (A.4) and (A.7) gives

$$\frac{\partial u_0}{\partial x} = \frac{N}{E_0} - \frac{E_1}{E_0}\frac{\partial \theta}{\partial x} \tag{A.8}$$

$$M = \left(E_2 - \frac{E_1^2}{E_0}\right)\frac{\partial \theta}{\partial x} + \frac{E_1}{E_0}N. \tag{A.9}$$

Next, insertion of Eq. (A.9) together with Eq. (A.5) into Eqs. (6) and (11) yields the desired coupled Eqs. (14) and (15).

References

[1] S. Suresh, A. Mortensen, *Fundamentals of Functionally Graded Materials*, ASM International and The Institute of Materials, Cambridge, 1995.

[2] B. Kieback, A. Neubrand, H. Riedel, Processing techniques for functionally graded materials, *Material Science and Engineering A* 362 (2003) 81–106.

[3] B.V. Sankar, An elasticity solution for functionally graded beams, *Composites Science and Technology* 61 (2001) 689–696.

[4] M. Aydogdu, V. Taskin, Free vibration analysis of functionally graded beams with simply supported edges, *Materials and Design* 28 (2007) 1651–1656.

[5] A. Chabraborty, S. Gopalakrishnan, J.N. Reddy, A new beam finite element for the analysis of functionally graded materials, *International Journal of Mechanical Science* 45 (2003) 519–539.

[6] Z. Zhong, T. Yu, Analytical solution of a cantilever functionally grade beam, *Composites Science and Technology* 67 (2007) 481–488.

[7] C.-F. Lu, W.Q. Chen, Free vibration of orthotropic functionally graded beams with various end conditions, *Structural Engineering and Mechanics* 20 (2005) 465–476.

[8] S.P. Timoshenko, On the transverse vibrations of bars of uniform cross-section, *Philosophical Magazine* 43 (1922) 125–131.

[9] R.Y. Cheng, Vibration of Timoshenko beams and frameworks, *ASCE Journal of Structural Division* 96 (1970) 551–571.
[10] W.P. Howson, F.W. Williams, Natural frequencies of frames with axially loaded Timoshenko members, *Journal of Sound and Vibration* 26 (1973) 503–515.
[11] H. Abramovich, I. Elishakoff, Application of the Krein's method for determination of natural frequencies of periodically supported beam based on simplified Bresse–Timoshenko equations, *Acta Mechanica* 66 (1987) 39–59.
[12] K. Chandrashekhara, K. Krishnamurthy, S. Roy, Free vibration of composite beams including rotary inertia and shear deformation, *Composite Structures* 14 (1990) 269–279.
[13] G. Oliveto, Dynamic stiffness and flexibility functions for axially strained Timoshenko beams, *Journal of Sound and Vibration* 154 (1992) 1–23.
[14] W.Q. Chen, C.F. Lv, Z.G. Bian, Elasticity solution for free vibration of laminated beams, *Composite Structures* 62 (2003) 75–82.
[15] A.M. Horr, L.C. Schmidt, Closed-form solution for the Timoshenko beam theory using a computer-based mathematical package, *Computers and Structures* 55 (1995) 405–412.
[16] J.R. Banerjee, Frequency equation and mode shape formulae for composite Timoshenko beams, *Composite Structures* 51 (2001) 381–388.
[17] T.C. Huang, The effect of rotatory inertia and of shear deformation on the frequency and normal mode equation beams with simple end conditions, *ASME Journal of Applied Mechanics* 28 (1961) 579–584.
[18] A.M. Chervyakov, V.V. Nesterenko, Is it possible to assign physical meaning to field theory with higher derivatives?, *Physical Review D* 48 (1993) 5811–5817.
[19] N.G. Stephen, The second spectrum of Timoshenko beam theory—further assessment, *Journal of Sound and Vibration* 292 (2006) 372–389.
[20] C.M. Wang, Timoshenko beam-bending solutions in terms of Euler–Bernoulli solutions, *Journal of Engineering Mechanics* 121 (1995) 763–765.
[21] J.F. Doyle, *Wave Propagation in Structures*, Springer, New York, 1989.
[22] C.R. Fuller, S.J. Elliott, P.A. Nelson, *Active Control of Vibration*, Academic, London, 1996.
[23] M. Levinson, D.W. Cooke, On the two frequency spectra of Timoshenko beams, *Journal of Sound and Vibration* 84 (1982) 319–326.
[24] K.T. Chan, X.Q. Wang, R.M.C. So, S.R. Reid, Superposed standing waves in a Timoshenko beam, *Proceedings of Royal Society London A* 458 (2002) 83–108.
[25] B. Geist, J.R. McLaughlin, Double eigenvalues for the uniform Timoshenko beam, *Applied Mathematics Letters* 10 (1997) 129–134.
[26] E. Kausel, Nonclassical modes of unrestrained shear beams, *Journal of Engineering Mechanics* 128 (2002) 663–667.
[27] N.F.J. van Rensberg, A.J. van der Merwe, Natural frequencies and modes of a Timoshenko beam, *Wave Motion* 44 (2006) 58–69.
[28] X.-F. Li, S.-H. Guo, Effects of nonhomogeneity on dynamic stress intensity factors for an anti-plane interface crack in a functionally graded material bonded to an elastic semi-strip, *Computational Material Science* 38 (2006) 432–441.
[29] A.J. Markworth, K.S. Ramesh, W.P. Parks Jr., Modelling studies applied to functionally graded materials, *Journal of Material Science* 30 (1995) 2183–2193.
[30] M. Grujicic, H. Zhao, Optimization of 316 stainless steel/alumina functionally graded material for reduction of damage induced by thermal residual stresses, *Material Science Engineering A* 252 (1998) 117–132.